Bioorganic & Medicinal Chemistry 27 (2019) 4059–4068

Contents lists available at ScienceDirect

Bioorganic & Medicinal Chemistry

journal homepage: www.elsevier.com/locate/bmc

Molecular modelling, synthesis, and biological evaluations of a 3,5-disubstituted isoxazole fatty acid analogue as a PPARα-selective agonist

Henriette Arnesen[a], Nadia Nabil Haj-Yasein[a], Jørn E. Tungen[b], Helen Soedling[a], Jason Matthews[a], Steinar M. Paulsen[c], Hilde I. Nebb[a], Ingebrigt Sylte[d], Trond Vidar Hansen[b], Thomas Sæther[a,e,*]

[a] Department of Nutrition, Institute of Basic Medical Sciences, University of Oslo, N-0317 Oslo, Norway
[b] Section of Pharmaceutical Chemistry, Department of Pharmacy, University of Oslo, N-0316 Oslo, Norway
[c] MabCent-SFI, UiT – The Arctic University of Norway, N-9037 Tromsø, Norway
[d] Department of Medical Biology, Faculty of Health Sciences, UiT – The Arctic University of Norway, N–9037 Tromsø, Norway
[e] Department of Molecular Medicine, Institute of Basic Medical Sciences, University of Oslo, N-0317 Oslo, Norway

ARTICLE INFO

InChIKeys:
QJMRNGLYZDICBV-LMJZYCSTSA-N
RDTXFVJNJHAAER-UHFFFAOYSA-N
DMLLBQUVTVEKCS-RSGUCCNWSA-N
WCRFOAMFVUQHMK-NBYYMMLRSA-N

Keywords:
Peroxisome proliferator activated receptor
Agonist
Oxohexadecenoic acid
Isoxazole
Lipid-lowering
Microalgae
Chaetoceros karianus

ABSTRACT

The peroxisome proliferator activated receptors (PPARs) are important drug targets in treatment of metabolic and inflammatory disorders. Fibrates, acting as PPARα agonists, have been widely used lipid-lowering agents for decades. However, the currently available PPARα targeting agents show low subtype-specificity and consequently a search for more potent agonists have emerged. In this study, previously isolated oxohexadecenoic acids from the marine algae *Chaetoceros karianus* were used to design a PPARα-specific analogue. Herein we report the design, synthesis, molecular modelling studies and biological evaluations of the novel 3,5-disubstituted isoxazole analogue 6-(5-heptyl-1,2-oxazol-3-yl)hexanoic acid (**1**), named ADAM. ADAM shows a clear receptor preference and significant dose-dependent activation of PPARα (EC_{50} = 47 μM) through its ligand-binding domain (LBD). Moreover, ADAM induces expression of important PPARα target genes, such as *CPT1A*, in the Huh7 cell line and primary mouse hepatocytes. In addition, ADAM exhibits a moderate ability to regulate PPARγ target genes and drive adipogenesis. Molecular modelling studies indicated that ADAM docks its carboxyl group into opposite ends of the PPARα and -γ LBD. ADAM interacts with the receptor-activating polar network of amino acids (Tyr501, His447 and Ser317) in PPARα, but not in PPARγ LBD. This may explain the lack of PPARγ agonism, and argues for a PPARα-dependent adipogenic function. Such compounds are of interest towards developing new lipid-lowering remedies.

1. Introduction

The peroxisome proliferator-activated receptors (PPARs) are ligand-activated nuclear receptors (NRs) with crucial roles in regulation of genes involved in a wide range of physiological processes. The PPARs respond to endogenous ligands, such as metabolites of fatty acids, or synthetic compounds.[1–3] In response to ligand binding, the PPARs heterodimerize with retinoid X receptor (RXR) and act on specific PPAR response elements (PPREs) in chromatin. Ligand binding initiates conformational changes in the LBD that facilitates dissociation or recruitment of transcriptional co-regulators, mainly carried out by the ligand-dependent activation function 2 (AF2). In addition, posttranslational modifications adjust the receptors' affinity for co-regulators and thereby determine whether a target gene is induced or repressed.[3–5] The PPARs are well known for their control of genes involved in lipid and glucose metabolism. Moreover, the PPARs are shown to encompass important roles in mediating biological effects related to inflammation and vascular function.[6–8]

The three PPAR subtypes identified in humans show a tissue specific expression. The subtypes PPARα and PPARγ are highly expressed in liver and adipose tissue, respectively, while PPARδ is more ubiquitously expressed.[9,10] Activation of PPARγ is essential for control of energy conservation through regulation of genes involved in lipogenesis and lipid storage.[11,12] In parallel, PPARα is the subtype most known for its effects in fatty acid disposal pathways. Through regulation of target genes involved in fatty acid transport, activation and oxidation, PPARα increases lipid uptake and energy expenditure in the liver.[13,14]

Given their key roles in multiple metabolic and inflammatory

* Corresponding author at: Department of Molecular Medicine Institute of Basic Medical Sciences, University of Oslo, N-0317 Oslo, Norway.
E-mail address: thomas.sather@medisin.uio.no (T. Sæther).

https://doi.org/10.1016/j.bmc.2019.07.032
Received 29 May 2019; Received in revised form 15 July 2019; Accepted 18 July 2019
Available online 19 July 2019

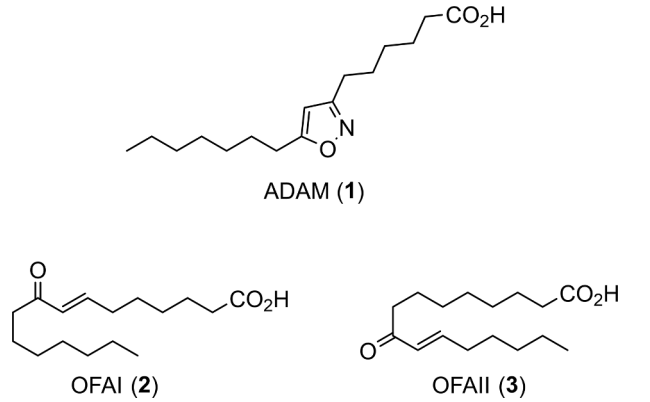

Fig. 1. Chemical structures of OFAI (**2**) and OFAII (**3**) and the synthetic isoxazole ADAM (**1**).

pathways, the PPARs are attractive targets for treatment of various metabolic disorders, such as the metabolic syndrome and type 2 diabetes mellitus. These disorders are strongly associated with atherogenic dyslipidaemia and increased risk of cardiovascular diseases (CVDs).[15] Collectively, CVDs comprise the main cause of death among these patients,[16] and thus therapeutic approaches toward these disorders aim to reduce modifiable risk factors. A group of widely used lipid-lowering drugs in this context is the fibrates, which act as PPARα agonists.[17] Fibrates and other PPARα agonists effectively reduce levels of circulating triglycerides and increase levels of anti-atherogenic HDL-C in high-risk subjects.[18–22] However, fibrates are low-affinity ligands for PPARα, and currently available PPARα agonists generally show low subtype selectivity. Furthermore, the efficacy of these agonists is limited due to dose-related adverse effects.[23,24] Thus, efforts have been made to develop new PPARα agonists that show higher levels of selectivity and potency than the fibrates.[24,25]

We previously identified and isolated the two isomeric oxohexadecenoic acids (7E)-9-oxohexadec-7-enoic (OFAI, 2) and (10E)-9-oxohexadec-10-enoic acid (OFAII, **3**) from the marine microalga *Chaetoceros karianus* (Fig. 1). These compounds exhibited PPARα/γ dual agonist activity.[26,27]

We used these two natural occurring oxohexadecenoic acids for the design of a potent and selective PPARα agonist (Fig. 1). Both OFAI and OFAII contain a α,β-unsaturated ketone moiety exhibiting putative cytotoxic effects as Michael acceptors. Such effects have been reported by oxo-fatty acids towards PPARγ.[28–30] One possible bioisosteric substitution for the Michael-acceptor is the 3,5-disubstituted isoxazole ring (Fig. 1). In this paper we report the synthesis, extensive biological evaluation and molecular modelling studies of this first generation analogue 6-(5-heptyl-1,2-oxazol-3-yl)hexanoic acid, named ADAM (**1**).

2. Results and discussion

2.1. Chemistry

The synthesis of ADAM (**1**) began with the base catalysed condensation of 1-nonyne (**4**) with methyl nitroacetate (**5**) affording isoxazole **6** in 73% yield, see Scheme 1. The methyl ester in **6** was then reduced to the corresponding aldehyde using diisobutylaluminium hydride (DIBAL-H). The freshly synthesized aldehyde was subsequently reacted in a Wittig olefination reaction with the ylide of commercially available (4-carboxybutyl)triphenylphosphonium bromide (**8**), the latter formed from the reaction with two equivalents of lithium *bis* (trimethylsilyl)amide (LiHMDS). This provided the alkenoic acid **9** in 64% yield over the two steps. Quantitative hydrogenation over palladium on carbon of **9** finalized the synthesis of ADAM (**1**). The spectroscopic data were in agreement with the chemical structure (Supporting information).

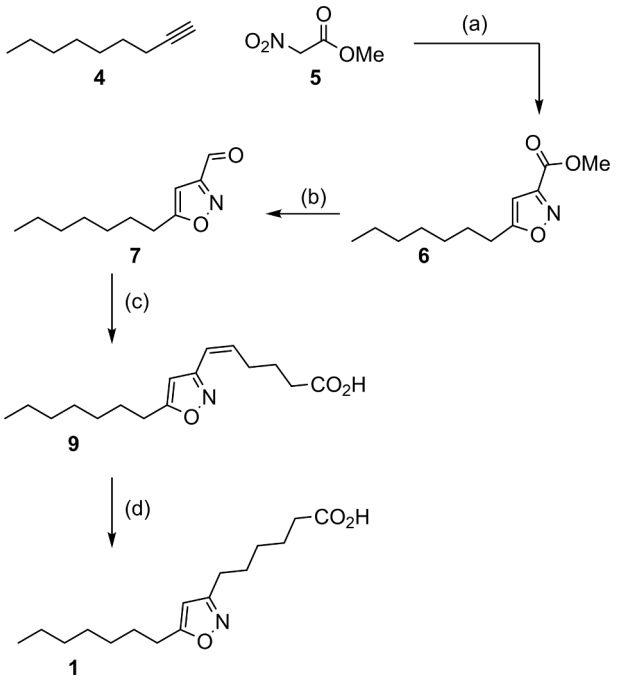

Scheme 1. Synthesis of ADAM. (a) DABCO, EtOH, 80 °C, 73 h; (b) DIBAL-H, dry CH_2Cl_2, −78 °C, 6 h; (c) LiHMDS, $BrPh_3P(CH_2)_4CO_2H$ (**8**), THF, −78 °C to rt, 18 h; (d) H_2, Pd/C, EtOAc, 12 h.

2.2. Docking studies

Docking of ADAM (**1**), OFAI (**2**) and OFAII (**3**) into the PPARα LBD gave VLS (virtual ligand screening) scoring values in the range of −35.1 to −29.4 for all compounds, and showed that the carboxylic group of all three compounds interacts with a hydrogen bonding network of polar amino acids that includes Ser280, Tyr314, His440, and Tyr464 (Fig. 2A, B). In the highest scored docking pose, the oxygen atom of the carbonyl group of ADAM forms hydrogen bonds with Ser280 (2.1 Å), Tyr314 (2.2 Å), Tyr464 (3.2 Å) and His440 (3.4 Å), while the hydroxyl group is located within a network of Tyr464 (3.7 Å), His440 (3.3 Å), Tyr464 (3.6 Å) and Tyr414 (3.5 Å) (Fig. 2B). The carbonyl oxygen of OFAI forms hydrogen bonds with Ser280 (2.2 Å), Tyr314 (2.1 Å), His 440 (3.4 Å) and Tyr464 (3.2 Å), while the hydroxyl group is located closest to Tyr464 (3.6 Å) and His440 (3.4 Å). The oxygen carbonyl of OFAII is involved in a hydrogen bonding network with Ser280 (2.1 Å), Tyr314 (2.2 Å), Tyr464 (3.2 Å) and His440 (3.4 Å), while the hydroxyl group is closest to Tyr464 (3.1 Å) (Fig. 2A).

Docking of the compounds into PPARγ showed poses quite similar to the PPARα poses (Fig. 2C, D). In addition, binding poses with the carboxylic group in the direction of Arg316 and Glu323 were observed for all compounds. For ADAM, this pose obtained the most favorable scoring value (-26.0 in the 2VST structure), with the carbonyl oxygen 1.6 Å from the side chain of Arg316 and the hydroxyl hydrogen 2.0 Å from the side chain of Glu323 (Fig. 2D). For OFAI/II poses similar to the orientation in PPARα were dominating with interactions between the carboxylic group oriented into the polar network of Ser317, His351, His477, Tyr355 and Tyr501 (Fig. 2C). The corresponding scoring value was −26.1 for OFAI (in the 2VVO structure) and −27.7 for OFAII (in the 2VV4 structure). The carbonyl oxygen of OFAI forms a hydrogen bond with His477 (1.6 Å), while the hydroxyl oxygen participates in a hydrogen bond with the side chain of Ser317 (1.8 Å), and the hydroxyl hydrogen forms a hydrogen bond with the side chain of His351 (2.3 Å) and Tyr501 (3.4 Å). The carbonyl oxygen of OFAII forms a hydrogen bond with Ser317 (1.6 Å), while the hydroxyl group donates a hydrogen bond to Tyr501 (2.1 Å), His477 (2.9 Å) and is acceptor for a hydrogen bond from His477 (1.7 Å). It seems like the binding of OFAI to PPARγ is

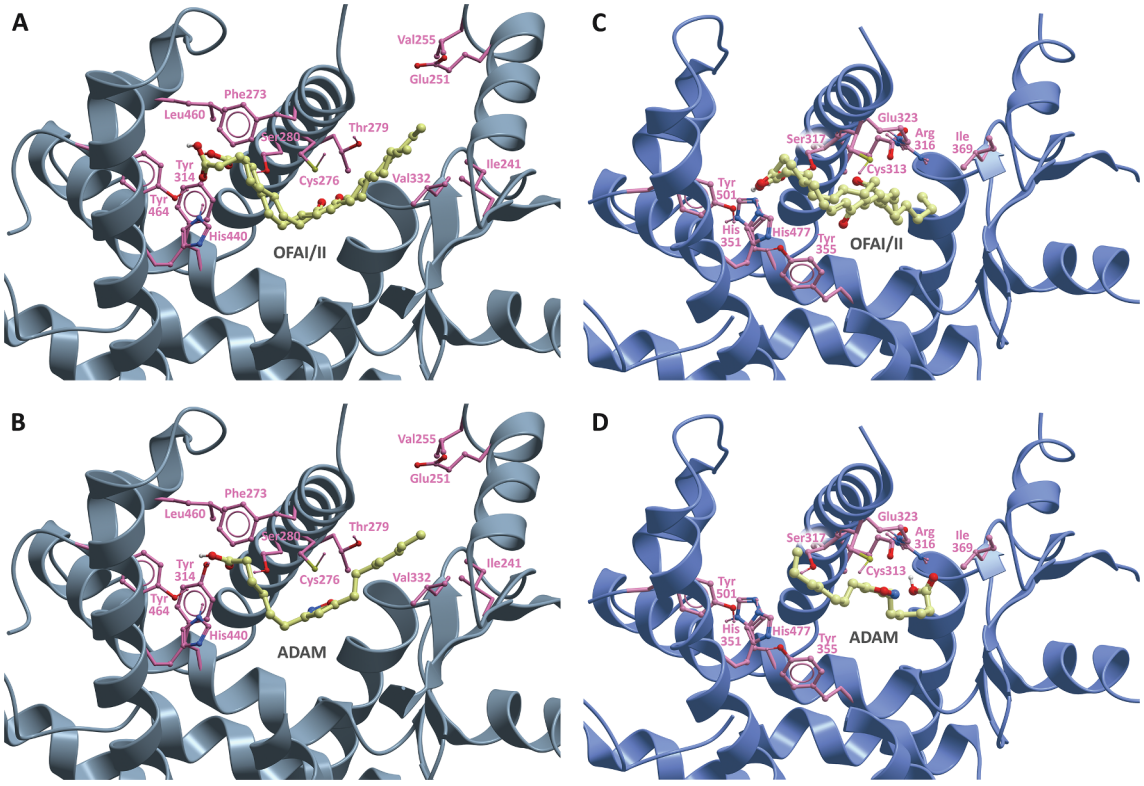

Fig. 2. ADAM, OFAI and OFAII docked into the LBD X-ray crystal structures of PPARα and PPARγ. Binding mode of the oxohexadecenoic acids OFAI and OFAII, and the analogue ADAM after docking into the ligand-binding domain of human PPARα (**A, B**; PDB entry 2P54) and PPARγ (**C, D**; PDB entry 2VV0). The figure shows the superposition of receptor–ligand complexes where the X-ray structures of the PPARs are shown as ribbon representation (PPARα in grey and PPARα in blue). Ball and stick models are used for the ligands (carbon-yellow, nitrogen-blue, oxygen-red, hydrogen-white) and central side groups (carbon and hydrogen-pink, nitrogen-blue, oxygen-red).

stabilized by shorter hydrogen bonds to the polar network than the binding to PPARα.

2.3. Biological assays

2.3.1. Dose-response and cytotoxicity

In order to assess the agonist activity and specificity of ADAM (**1**), we performed dual-luciferase assays with GAL4 tethering constructs where the LBD of different nuclear receptors were fused in frame with GAL4 DNA-binding domain (DBD), enabling us to compare the ADAM agonist activity from different NRs on the same GAL4-responsive luciferase reporter. Cytotoxicity was determined simultaneously by measurement of lactate dehydrogenase (LDH) in cell media. In addition, cytotoxicity was assessed in standard XTT-based assays.

These experiments revealed that ADAM displayed a sigmodial dose-response with respect to PPARα agonist activity, and an EC_{50} value of 47 μM (Fig. 3A). Given that the parent compounds are dual PPARα/γ agonists and that ADAM showed a relatively high docking score for PPARγ, we also assessed whether ADAM could activate PPARγ. As can be seen from Fig. 3B, a minor induction of PPARγ activity was observed at concentrations in the millimolar range, with an estimated EC_{50} value of 2.0 mM. This indicated a lack of PPARγ agonism.

Cell viability decreased at concentrations of 10^{-4} M ADAM in both LDH and XTT assays (Fig. 3C, D), with rapid reduction to respectively 60 % and 40 % at 10^{-3} M.

Since ADAM had low to no activity towards PPARγ, while docking indicated PPARγ binding, we also assayed its ability to act as a neutral or inverse agonist [31] by allowing it to compete with the classical PPARγ agonist Rosiglitazone. As can be seen from Fig. 4, even the highest millimolar concentrations of ADAM was unable to outcompete 1.0 μM Rosiglitazone.

2.3.2. Selective PPARα agonist activity

To assess the selectivity of ADAM with respect to nuclear receptor agonist activity, we transfected COS-1 cells with GAL4-LBD fusion constructs of different nuclear receptors LBDs, and treated them with increasing concentrations of ADAM. The ADAM concentrations applied were based on the empirical EC_{50} values determined previously (Fig. 3).

As expected, human PPARα activity was significantly induced upon treatment with both 25 and 50 μM ADAM (Fig. 5). A minor PPARδ and –γ agonist activity were observed, but the induction was not significant in the model used. ADAM activated none of the other NR-LBD fusion proteins under these conditions. The in vitro cell-based reporter assays revealed that ADAM behaved as a specific PPARα agonist. When compared to the known PPARα agonist Pirinixic acid, ADAM demonstrated an about 2.5-fold greater efficacy in activating PPARα (Fig. 6).

We proceeded to evaluate the ability of ADAM to activate natural PPARα- and PPARγ-regulated promoters, in order to study the agonist activity in a more relevant context. ADAM was able to significantly activate the PPARα target gene promoter *CPT1A* (Fig 7A), but not the PPARγ target gene promoter *PLIN1* (Fig. 7B). The *CPT1A* activation was dependent on both full-length PPARα and a functional PPRE.

2.3.3. Activation of endogenous PPARα target genes in hepatocytes

To investigate the effects of ADAM on endogenous, chromatinized PPAR target genes, we used two separate hepatocyte models; the human hepatocellular carcinoma cell line Huh7 and primary mouse hepatocytes. Of all the genes analysed, the induction of *CPT1A/Cpt1a* expression was the most prominent. As can be seen from Fig. 8, this gene was significantly upregulated by ADAM, comparable to the PPARα agonists Pirinixic acid and GW7647, both in Huh7 cells and primary mouse hepatocytes. The relative expressions of *PPARA, SCD and SREBF1* were unaffected by any of the treatment in Huh7 cells.

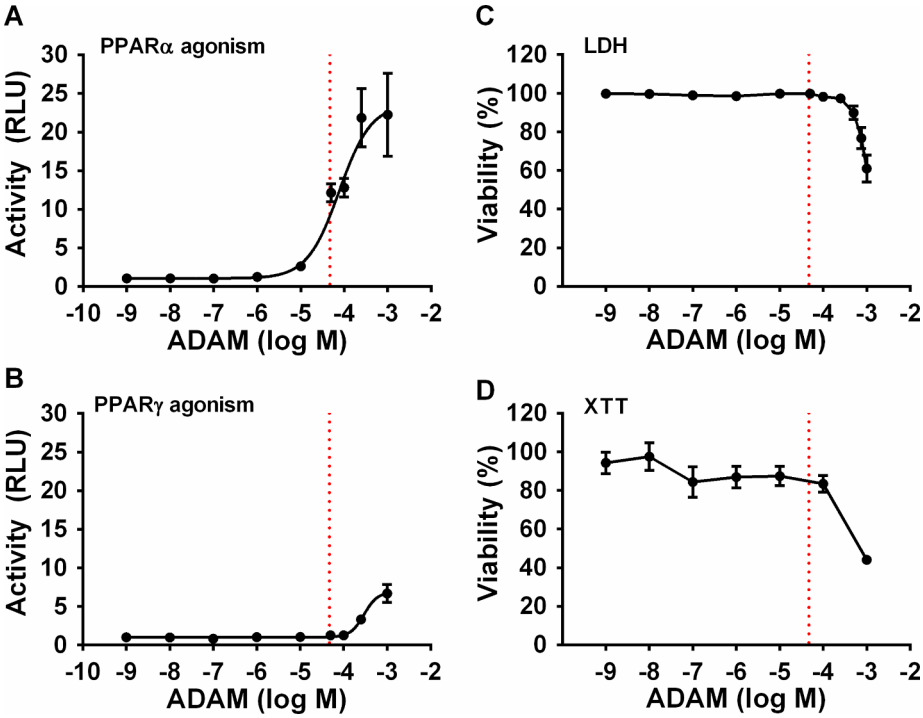

Fig. 3. ADAM activates PPARα and displays low cytotoxicity at EC_{50}. The assays were run with GAL4-DBD-NR-LBD chimeric constructs in COS-1 cells, using LBD from human PPARα and PPARγ, respectively. The graphs show the dose–response relationship for ADAM with respect to human PPARα (**A**) and PPARγ (**B**), normalized to the activity measured with empty vector (GAL4 only). Corresponding cytotoxicity data were obtained by measuring lactate dehydrogenase (LDH) in media or (**C**) by running XTT based assays (**D**). The data represent three biological replicates analysed in quadruplicates, and are presented as mean ± SEM. RLU, Relative light units. The stapled red lines indicate the EC_{50}-value for PPARα activation.

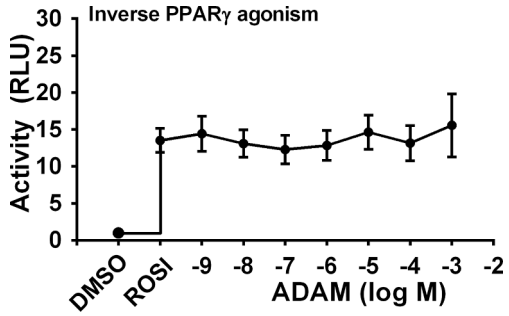

Fig. 4. ADAM is unable to outcompete Rosiglitazone in activation of PPARγ. The assays were run with GAL4-DBD-PPARγ-LBD chimeric construct in COS-1 cells. The graph shows the inverse PPARγ agonism dose–response for ADAM when titrated against 1.0 μM Rosiglitazone, normalized to the activity measured with empty vector (GAL4 only). The data represent three biological replicates analysed in quadruplicates, and are presented as mean ± SEM. RLU, Relative light units.

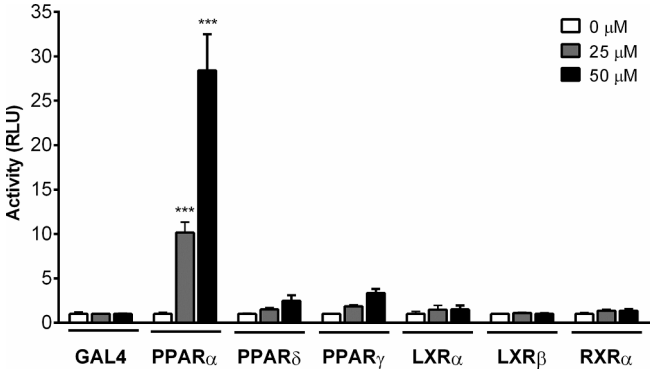

Fig. 5. ADAM shows agonist activity specific for PPARα. The assays were run with GAL4-DBD-NR-LBD chimeric constructs in COS-1 cells, using the ligand binding domain (LBD) from human nuclear receptors. The cells were treated with 0, 25 or 50 μM of ADAM dissolved in DMSO (final concentration 0.1 %), as indicated in the legend. The data represent three biological replicates analysed in quadruplicates, normalized to respective DMSO control (0 μM) and GAL4, and are presented as mean ± SEM. Statistical differences were analyzed using two-way ANOVA followed by Bonferroni's correction for multiple comparisons. Adjusted p-value $^{***}p \leq 0.001$ compared to DMSO (0 μM ADAM) control. RLU, Relative light units.

However, in primary mouse hepatocytes *Scd1* and *Srebf1* were significantly induced by ADAM, which grouped together with the other PPARα agonists GW7647 and Pirinixic acid. The parental oxohexadecenoic acids OFAI (**2**) and OFAII (**3**) seemed to group with Rosiglitazone and induced the expression of *Ppara* while having no effect on the *Scd1* and *Srebf1* expression in primary mouse hepatocytes. This is in line with what we have observed earlier for the OFAs in Huh7.[27]

2.3.4. Adipocyte differentiation

We continued to study the activation of adipocyte-specific PPAR target genes, using the human Simpson-Golabi-Behmel syndrome (SGBS) pre-adipocyte cell line.[32] By exchanging the PPARγ-agonist Rosiglitazone, which is an essential component in the differentiation medium, with ADAM, Pirinixic acid, OFAI, OFAII or DMSO, we could evaluate the compound's effects on target gene activation and cell morphology changes. As expected, Rosiglitazone induced the expression of most PPARγ target genes during the course of differentiation (Fig. 9). Surprisingly, ADAM also induced expression of genes involved in adipogenic differentiation (*PPARG*, *CEBPA*), lipid metabolism and storage (*ACSL1*, *CD36*, *FABP4*, *PLIN1*) and adipokine expression (*ADIPOQ*, *ANGPTL4*). On a general basis, the effect of ADAM on relative expression levels of PPARγ target genes appears similar to that of Pirinixic acid, lower than Rosiglitazone, and higher than OFAI and -II.

To evaluate the effects of ADAM on adipocyte differentiation at the morphological level, we stained the treated SGBS cells with Oil Red O. Rosiglitazone was, as anticipated, the most potent promoter of lipid droplet formation, i.e. adipocyte differentiation, although Pirinixic acid also exhibited a clear adipogenic potential (Fig. 10). Mirroring what was observed at the gene expression level, ADAM seems to promote adipocyte differentiation to a higher extent than OFAI and –II, but to a considerably lesser extent than both Rosiglitazone and Pirinixic acid (Fig. 10).

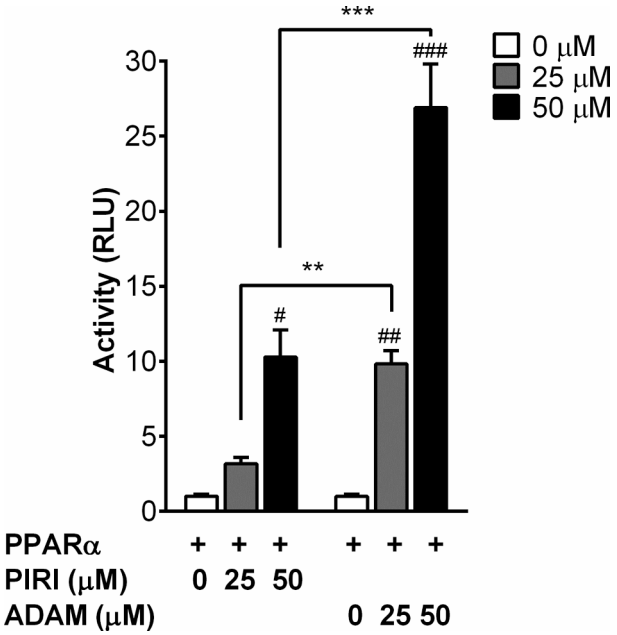

Fig. 6. ADAM demonstrates a greater efficacy in activating PPARα than Pirinixic acid. The assays were run with GAL4-DBD-PPARα-LBD chimeric constructs in COS-1 cells. The cells were treated with 0, 25 or 50 μM of ADAM or Pirinixic acid (PIRI) dissolved in DMSO (final concentration 0.1 %), as indicated in the legend. The Luciferase activity data, representing three biological replicates analysed in quadruplicates, were normalized to GAL4 empty vector and DMSO control, and presented as mean ± SEM. Statistical differences were analyzed using two-way ANOVA followed by Bonferroni's correction for multiple comparisons. Significant differences in PPARα activation are denoted by asterisks (*) for ADAM versus Pirinixic acid treatment, and hash (#) for treated (25/50 μM) versus respective untreated groups (0 μM). Adjusted p-values $^{**}p \le 0.01$, $^{***}p \le 0.001$, $^{\#}p \le 0.05$, $^{\#\#}p \le 0.01$, $^{\#\#\#}p \le 0.001$. RLU, Relative light units.

Although PPARγ is the PPAR subtype predominantly expressed in white adipocytes, the effects observed upon ADAM and Pirinixic acid treatment in this study indicates a function for PPARα in these cells. The role of PPARα in white adipose tissue (WAT) is still not fully understood, but previous studies have pointed towards an involvement in WAT metabolism and differentiation.[33–35] Induction of *ADIPOQ* expression in mouse WAT and human subjects with PPARα agonists have previously been reported.[36] Goto et al. [37] have shown that PPARα activation induced adipocyte differentiation with limited lipid accumulation in 3T3-L1 adipocytes as well as in mice WAT. They further hypothesized that PPARα are involved in driving adipocyte hyperplasia but not hypertrophy.

The strong and continuous increase in PPARγ target expression observed upon Rosiglitazone treatment may be attributed to this agonist's ability to induce production of endogenous ligands. Increased levels of the CD36 scavenger receptor, which mediates uptake of lipid particles including oxidized LDL (oxLDL), could provide the cell with hydroxyoctadecadienoic acids (HODEs) and hydroxyeicosatetraenoic acids (HETEs) which are known PPARγ agonists and components of oxLDL.[38–40] Alternatively, induction of the rate-limiting enzyme in prostaglandin synthesis, COX2, could provide the cells with other natural ligands, like 15d-PGJ_2.[41,42] While ADAM might be able to drive some of these processes, another possibility is that metabolites produced in PPARα-mediated processes may activate PPARγ. Fatty acids induce their own breakdown through activation of PPARα.[43,44] As activated PPARα leads to upregulation of *CYP4A* which mediates ω-hydroxylation, metabolites produced during catabolism of PPARα ligands may in turn activate PPARγ.[45]

To discriminate between these alternative adipogenic functions of ADAM, more sophisticated experiments will have to be conducted, combining conditional knock-down of PPARα and PPARγ with agonist treatment in SGBS cells or preferably primary adipocytes from healthy donors. This is however beyond the scope of the current paper.

The X-ray crystal structures of receptor-agonist complexes show that the acidic head groups of the agonists form a hydrogen bonding network with a polar part of the LBD that includes amino acids such as Ser317, His351, Tyr355, His477 and Tyr501 in PPARγ.[46] These interactions are crucial for stabilizing the AF2 domain in a conformation for coactivator binding and receptor activation. The PPARα docking indicates that ADAM, OFAI and OFAII form a hydrogen bonding network with the corresponding network of polar amino acids (Fig. 2A and B). However, in PPARγ the docking also indicated an alternative binding pose with the polar head group interacting strongly with Arg316 and Glu323 (Fig. 2C and D). These amino acids form a strong polar region close to the part of the LBD where the agonist's aliphatic tail usually interacts. PPARα has a threonine (Thr279) at a position corresponding to Arg316 PPARγ, indicating that this area is less polar in PPARα than in PPARγ. For ADAM, the alternative pose was the best scored, indicating that the polar head group interacts with Arg316 and Glu323. This suggests that ADAM is not able to interact with the receptor-activating polar network of amino acids, and hence not able to stabilize the AF2 domain of PPARγ in a conformation for coactivator recruitment and receptor activation.[47] Taken together, this seems to be the most plausible explanation for the lack of PPARγ agonism and argues for a PPARα-dependent adipogenic function of the oxohexadecenoic acid analogue ADAM.

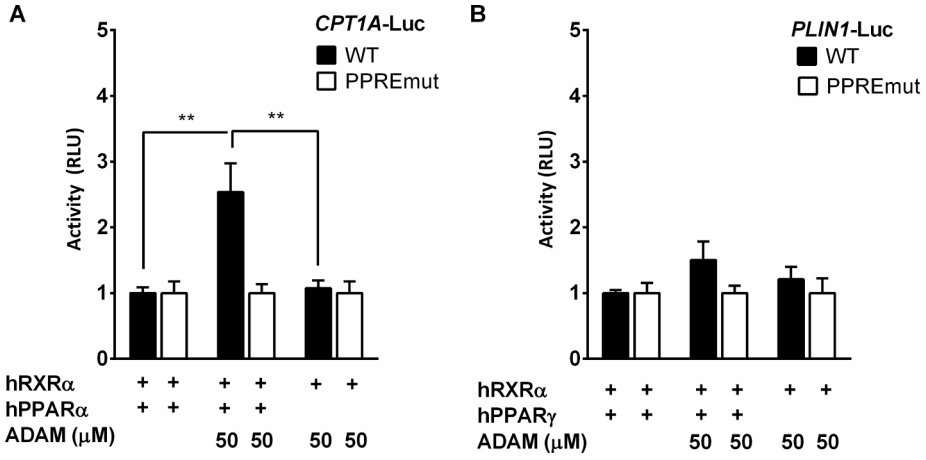

Fig. 7. ADAM activates human promoters in a PPARα/PPRE dependent fashion. COS-1 cells were transfected with plasmids expressing (**A**) full-length human PPARα, RXRα, and a *CPT1A*-driven reporter as wild-type (WT; black bars) or with mutated PPRE (white bars), or (**B**) full-length human PPARγ, RXRα, and *a PLIN1*-driven reporter as wild-type (black bars) or with mutated PPRE (white bars). The cells were treated with 50 μM ADAM dissolved in DMSO (final concentration 0.1 %). The Luciferase activity data, representing three biological replicates analysed in quadruplicates, were normalized to the DMSO control, and presented as mean ± SEM. Statistical differences were analyzed using two-way ANOVA followed by Bonferroni's correction for multiple comparisons. Differences between groups on the wild-type promoters are indicated by asterisks; adjusted p-values $^{**}p \le 0.01$. RLU, Relative light units.

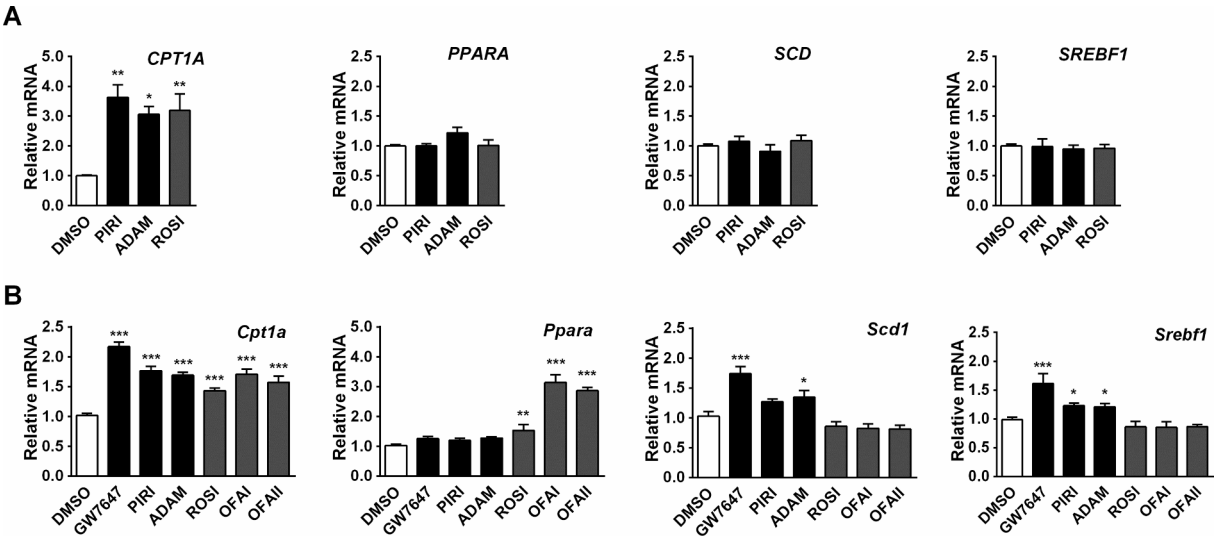

Fig. 8. ADAM activates endogenous PPARα target genes in (**A**) human hepatocarcinoma cells and (**B**) primary mouse hepatocytes. The cells were treated with 50 μM ADAM, 50 μM PIRI, 1 μM ROSI, 1 μM GW7647, 50 μM OFAI, or 50 μM OFAII for 18 hours before harvested for qPCR analysis. The data represent two biological replicates analysed in duplicates, normalized to the respective DMSO controls, and are presented as mean ± SEM. Statistical differences were analyzed using one-way ANOVA followed by Bonferroni's correction for multiple comparisons. Adjusted p-values $^{*}p \leq 0.05$, $^{**}p \leq 0.01$, and $^{***}p \leq 0.001$ compared to DMSO control. PIRI, Pirinixic acid; OFAI, (7*E*)-9-oxohexadec-7-enoic acid; OFAII, (10*E*)-9-oxohexadec-10-enoic acid; ROSI, Rosiglitazone.

3. Conclusions

Molecular modelling studies and pharmacological characterization of the novel synthetic 3,5-disubstituted isoxazole analogue 6-(5-heptyl-1,2-oxazol-3-yl)hexanoic acid ADAM (**1**) showed specific activation of PPARα. The molecular modelling experiments suggest that ADAM is unable to interact with the receptor-activating polar network of amino acids in PPARγ, necessary for AF2 stabilization and coactivator recruitment. However, ADAM regulates important PPAR target genes in both hepatocytes and adipocytes. Whether the apparent induction of adipocyte differentiation seen with ADAM in the SGBS model is due to PPARγ or PPARα-dependent target gene activation needs to be studied further. However, the molecular modelling analysis and data from specificity assays point in the direction of the latter.

4. Material and methods

4.1. General

Unless stated otherwise, all commercially available reagents and solvents were used in the form they were supplied without any further purification. The stated yields are based on isolated material. Melting points were measured using a Barnstead Electrothermal IA9200 melting point apparatus. Thin layer chromatography was performed on silica gel 60 F_{254} aluminum-backed plates fabricated by Merck. Flash column chromatography was performed on silica gel 60 (40–63 μm) produced by Merck. NMR spectra were recorded on a Bruker AVII400 or a Bruker DPX300 spectrometer at 400 MHz or 300 MHz respectively for ^{1}H NMR and at 100 MHz or 75 MHz respectively for ^{13}C NMR. Coupling constants (*J*) are reported in hertz and chemical shifts are reported in parts per million (δ) relative to the central residual protium solvent resonance in ^{1}H NMR ($CDCl_3$ = δ 7.27) and the central carbon solvent resonance in ^{13}C NMR ($CDCl_3$ = δ 77.00). Mass spectra and high resolution mass spectra were recorded at 70 eV on Micromass Prospec Q or Micromass QTOF 2 W spectrometer using ESI as the method of ionization.

4.2. Synthesis of compounds

4.2.1. Methyl 5-heptylisoxazole-3-carboxylate (6)

Methyl nitroacetate (**5**) (500 mg, 4.47 mmol) and 1-nonyne (**4**) (434 mg, 3.50 mmol) were dissolved in absolute EtOH (6.8 mL). DABCO (26.4 mg, 0.24 mmol) was added and the mixture was heated to 80 °C. After 72 h at 80 °C, the mixture was concentrated under vacuum. The crude product was purified by silica gel column chromatography (hexane-EtOAc 9:1). White solid (575 mg, 73%). m.p: 48–49 °C. ^{1}H NMR (400 MHz, Chloroform-*d*) δ 6.41 (s, 1H), 3.96 (s, 3H), 2.80 (t, *J* = 7.6 Hz, 2H), 1.71 (p, *J* = 7.5 Hz, 2H), 1.57–1.20 (m, 8H), 0.88 (t, *J* = 6.9 Hz, 3H). ^{13}C NMR (101 MHz, $CDCl_3$) δ 175.9, 160.7, 156.0, 101.4, 52.8, 31.6, 28.9, 28.8, 27.4, 26.7, 22.6, 14.0. R_f = 0.46; (EtOAc-hexane 3:7), HRMS (ESI): calculated $C_{12}H_{19}NO_3Na$: 248.1257, found: 248.1257.

4.2.2. 5-Heptylisoxazole-3-carbaldehyde (7)

A solution of ester **6** (300 mg, 1.33 mmol, 1.00 equiv.) in anhydrous CH_2Cl_2 (6.0 mL) was cooled to −78 °C under argon atmosphere and slowly treated over 5 minutes with a solution of diisobutylaluminum hydride (DIBAL-H) (1.62 mL, 1.0 M in CH_2Cl_2, 1.62 mmol, 1.20 equiv.). The reaction mixture was stirred at −78 °C for 6 h and then quenched with ice. A sat. aq. solution of Rochelle-salt (10 mL) was added. The phases were separated and the aq. phase was extracted with CH_2Cl_2 (3 × 10 mL). The combined organic layers were dried ($MgSO_4$), before it was concentrated *in vacuo*. The resultant residue was purified by silica gel column chromatography (hexane-EtOAc 9:1). Clear oil (220 mg, 81%). ^{1}H NMR (300 MHz, Chloroform-*d*) δ 10.12 (s, 1H), 6.37 (s, 1H), 2.81 (t, *J* = 7.6 Hz, 2H), 1.72 (p, *J* = 7.4 Hz, 2H), 1.43–1.21 (m, 8H), 0.88 (t, *J* = 6.4 Hz, 3H). ^{13}C NMR (101 MHz, $CDCl_3$) δ 185.3, 176.3, 162.3, 98.1, 31.8, 29.1, 29.0, 27.5, 26.8, 22.7, 14.2. R_f = 0.53; (hexane-EtOAc 8:2), HRMS (ESI): calculated $C_{11}H_{17}NO_3Na$: 218.1151, found: 218.1151.

4.2.3. (Z)-6-(5-heptylisoxazol-3-yl)hex-5-enoic acid (9)

To (4-carboxybutyl)triphenylphosphonium bromide (**8**) (545 mg, 1.23 mmol, 2.0 equiv.) in THF (20 mL) was added LiHMDS (2.46 mL,

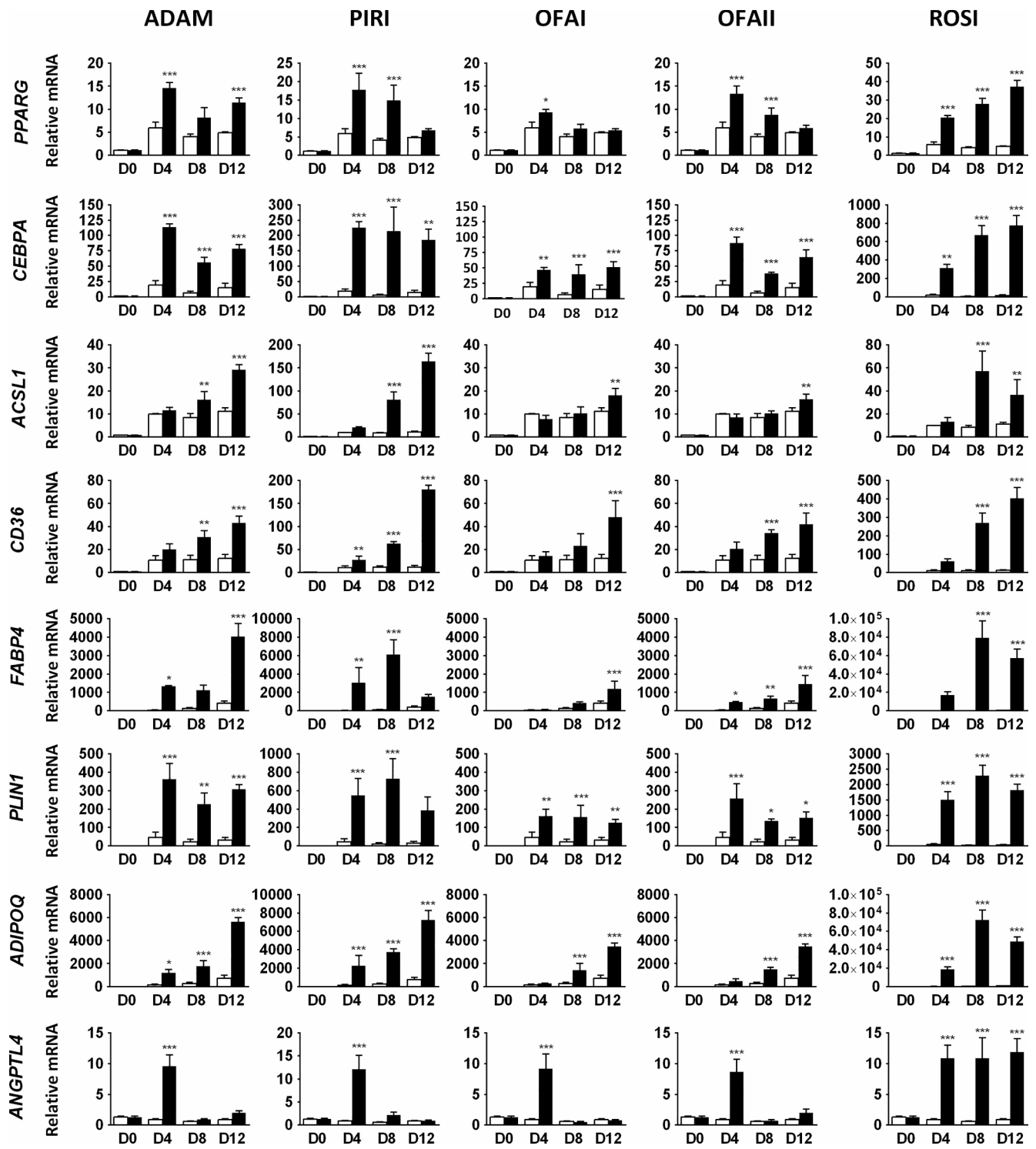

Fig. 9. ADAM activates endogenous PPARγ target genes in human adipocytes. Differentiation of SGBS cells was initiated with differentiation medium supplied with either 0.1 % DMSO (white bars), 25 μM ADAM, 25 μM OFAI, 25 μM OFAII, 25 μM PIRI, or 2 μM ROSI (black bars) on day 0, and gene expression measured by qPCR on day 0, 4, 8, and 12. The data represent minimum three biological replicates analysed in duplicates, normalized to day 0 (D0), and are presented as mean ± SEM. Statistical differences were analyzed using two-way ANOVA followed by Bonferroni's correction for multiple comparisons. Adjusted p-values $^{*}p \leq 0.05$, $^{**}p \leq 0.01$, and $^{***}p \leq 0.001$ compared to DMSO control for each time point. PIRI, Pirinixic acid; OFAI, (7*E*)-9-oxohexadec-7-enoic acid; OFAII, (10*E*)-9-oxohexadec-10-enoic acid; ROSI, Rosiglitazone.

1.0 M in THF, 4.0 equiv.) slowly at −78 °C. The solution was heated to room temperature and stirred for 30 min before being cooled to −78 °C again. Aldehyde **7** (120 mg, 0.61 mmol, 1.0 equiv.) in THF (5 mL) was added at −78 °C. The solution was allowed to slowly warm up to room temperature in a dry ice/acetone bath for 16 h before it was quenched with aq. NH_4Cl (15 mL). Et_2O (15 mL) was added and the phases were separated. The aqueous phase was extracted with Et_2O (2 × 15 mL) and the combined organic layers were washed with brine (20 mL), dried (Na_2SO_4) and then concentrated *in vacuo*. The resultant residue was purified by silica gel column chromatography (hexane-EtOAc 1:1).

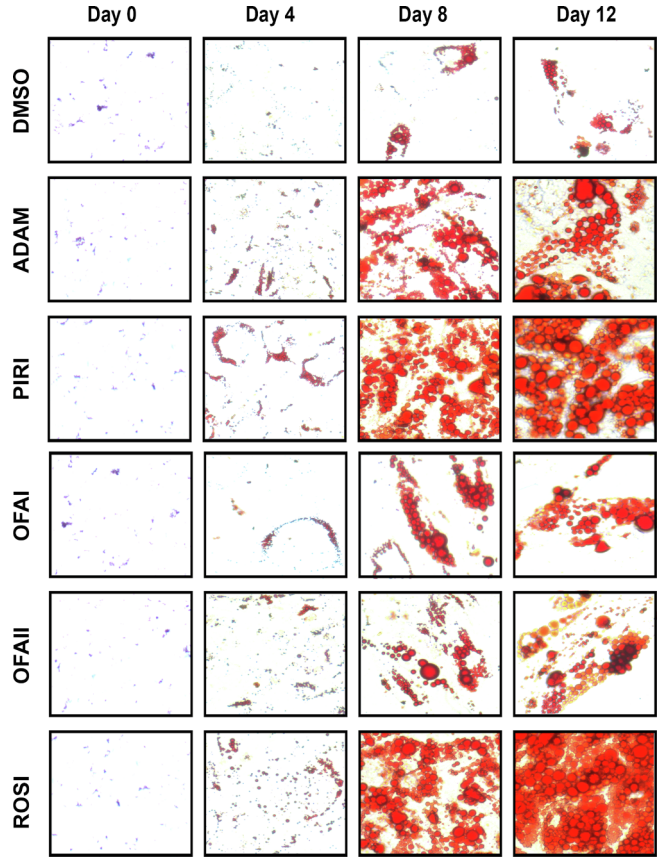

Fig. 10. ADAM drives accumulation of lipids in human adipocytes. Differentiation of SGBS cells was initiated with differentiation medium supplied with either 0.1 % DMSO, 25 μM ADAM, 25 μM OFAI, 25 μM OFAII, 25 μM PIRI, or 2 μM ROSI. The pictures show representative areas of wells with cells stained with Oil Red O at day 0, 4, 8, and 12 after onset of differentiation. PIRI, Pirinixic acid; OFAI, (7*E*)-9-oxohexadec-7-enoic acid; OFAII, (10*E*)-9-oxohexadec-10-enoic acid; ROSI, Rosiglitazone.

Clear oil at room temperature (solidifies in freezer) (136 mg, 79%). ^{1}H NMR (300 MHz, Chloroform-*d*) δ 9.50 (bs, 1H), 6.29 (dt, *J* = 11.6, 1.7 Hz, 1H), 5.99 (s, 1H), 5.91 (dt, *J* = 11.6, 7.4 Hz, 1H), 2.72 (t, *J* = 7.6 Hz, 2H), 2.51 (qd, *J* = 7.5, 1.7 Hz, 2H), 2.42 (t, *J* = 7.5 Hz, 2H), 1.82 (p, *J* = 7.5 Hz, 2H), 1.69 (p, *J* = 7.5 Hz, 2H), 1.41–1.19 (m, 8H), 0.92–0.83 (m, 3H). ^{13}C NMR (101 MHz, $CDCl_3$) δ 179.3, 173.5, 159.9, 137.6, 117.9, 101.3, 33.5, 31.8, 29.2, 29.0, 28.9, 27.7, 26.8, 24.3, 22.8, 14.2. R_f = 0.18; (CH_2Cl_2/MeOH 95:5), HRMS (ESI): calculated $C_{16}H_{25}NO_3Na$: 302.1727, found: 302.1727.

4.2.4. 6-(5-Heptyl-1,2-oxazol-3-yl)hexanoic acid (ADAM, 1)

10% Pd/C (5 mg) was added to a solution of the alkenoic acid **9** (40 mg, 0.14 mmol) in EtOAc (5 mL). The reaction flask was evacuated and flushed with H_2. This procedure was repeated three times. The mixture was stirred at room temperature for 12 h under H_2 and filtered through a pad of Celite. The filtrate was concentrated to give the saturated product. Pale beige solid (38 mg, 94%). m.p: 37–38 °C. ^{1}H NMR (400 MHz, Chloroform-*d*) δ 10.12 (bs, 1H), 5.80 (s, 1H), 2.68 (t, *J* = 7.7 Hz, 2H), 2.62 (t, *J* = 7.6 Hz, 2H), 2.35 (t, *J* = 7.5 Hz, 2H), 1.72–1.58 (m, 6H), 1.46–1.19 (m, 10H), 0.97–0.80 (m, 3H). ^{13}C NMR (101 MHz, $CDCl_3$) δ 179.6, 173.6, 163.8, 100.4, 34.0, 31.8, 29.2, 29.0, 28.7, 28.0, 27.6, 26.9, 26.0, 24.5, 22.7, 14.2. R_f = 0.18; (CH_2Cl_2/MeOH 95:5) HRMS (ESI): calculated $C_{16}H_{27}NO_3Na$: 304.1883, found: 304.1883.

4.3. Biological assays

4.3.1. Plasmids

The pSG5-GAL4, pSG5-GAL4-hPPARα-LBD, pSG5-GAL4-hPPARδ-LBD and pSG5-GAL4-hPPARγ-LBD, pSG5-GAL4-hLXRα-LBD, pSG5-GAL4-hLXRβ-LBD, and pSG5-GAL4-hRXRα-LBD plasmids encoding a GAL4 DNA-binding domain (DBD; aa 1-147) fused in frame with SV40 Nuclear localization signal 1 (NLS1), and LBD of human PPARα, PPARδ, PPARγ, LXRα, LXRβ, and RXRα have been described before.[27] The plasmids encoding FLAG-tagged full-length human PPARα, PPARγ, and RXRα have been described earlier.[26,48] The pGL3-5 × UAS-SV40 luciferase reporter, as well as the human PLIN1-driven reporters, pGL3-hPLIN1-3′del and pGL3-hPLIN1-3′del PPREmut, have also been previously described.[11,26] The human CPT1A-driven reporters, pGL3-hCPT1AInt and pGL3-hCPT1AInt PPREmut, were received as a gift from Prof. Diego Haro Bautista and have been described previously.[49] The vector pRL-CMV (Promega, Madison, WI), constitutively expressing Renilla Luciferase, was used as a control of transfection efficiency. All cloned plasmids have been sequenced, and cloning primer sequences are available upon request.

4.3.2. Cell culture

COS-1 cells were maintained in high glucose Dulbecco's modified Eagle's medium (DMEM; Sigma-Aldrich, #D6546) enriched with 10 % heat-inactivated fetal bovine serum (FBS; Sigma-Aldrich, #F7524), 4 mM L-Gln (Sigma-Aldrich, #G7513) and 50 U/mL penicillin/50 μg/mL streptomycin (Sigma-Aldrich, #P4458) at 37 °C in a humidified atmosphere of 5 % CO_2 in air. Cell confluence never exceeded 80 % prior to sub-culturing or transfection.

HuH-7 cells were maintained in high glucose DMEM (Sigma-Aldrich, #D6546) enriched with 10 % heat-inactivated FBS (Sigma-Aldrich, #F7524), 4 mM L-Gln (Sigma-Aldrich, #G7513), 50 U/mL penicillin/50 μg/mL streptomycin (Sigma-Aldrich, #P4458) and ITS (10 ng/mL insulin, 5.5 ng/mL transferrin, 5 pg/mL selenium; Sigma-Aldrich, #I3146) at 37 °C in a humidified atmosphere of 5 % CO_2 in air.

Human Simpson-Golabi-Behmel Syndrome (SGBS) cells were cultured in DMEM/Nutrient Mix F12 Ham (Sigma-Aldrich, #D6421) with 10 % non-inactivated FBS (Sigma-Aldrich, #F7524), 4 mM L-Gln (Sigma-Aldrich, #G7513), and 50 U/mL penicillin/50 μg/mL streptomycin (Sigma-Aldrich, #P4458), supplemented with a vitamin mix of 8 mg/mL biotin (Sigma-Aldrich, #B4639) and 4 mg/L D-pantotenate (Sigma-Aldrich, #P5155), for 4 days prior to differentiation. The SGBS cells were differentiated into adipocytes as previously described.[32] To initiate differentiation, medium was changed to a culture medium without FBS, supplemented with human 0.01 mg/mL apo-transferrin (Sigma-Aldrich, #T4382), 20 nM human insulin (Sigma-Aldrich, #I2643), 0.2 nM triiodythyronine (Sigma-Aldrich, #T6397), 100 nM hydrocortisol (Sigma-Aldrich, #D2915), 500 μM IBMX (Sigma-Aldrich, #I5879) and 25 nM dexamethasone (Sigma-Aldrich, #D2915), with addition of 25 μM ADAM, 25 μM Pirinixic acid (PIRI; WY-14643; C7081, Sigma-Aldrich) 25 μM (7E)-9-oxohexadec-7-enoic (OFAI), 25 μM (10E)-9-oxohexadec-10-enoic acid (OFAII), 2 μM Rosiglitazone (ROSI; BRL-49653, Cayman chemical, Ann Arbor, MI), or 0.1 % DMSO. After 4 days, medium was changed to a culture medium without FBS, supplemented with human 0.01 mg/mL apo-transferrin (Sigma-Aldrich, #T4382), 20 nM human insulin (Sigma-Aldrich, #I2643), 0.2 nM triiodythyronine (Sigma-Aldrich, #T6397), 100 nM hydrocortisol (Sigma-Aldrich, #D2915), that was renewed at day 8. The culture was terminated at day 12. Cells were harvested for RNA isolation and stained with Oil Red O at day 0, 4, 8, and 12.

4.3.3. Primary hepatocytes

All animal use was approved and registered by the Norwegian Animal Research Authority. Mice were housed in a temperature

controlled (22 °C) facility with a strict 12 h light/dark cycle. Male C57BL/6N mice (Jackson Laboratory) aged 7–8 weeks were used to isolate primary hepatocytes. Mice were first anaesthetised with isoflurane (AbbVie) and then their livers were perfused via the portal vein with liver perfusion medium (Thermo Fisher Scientific, #17701038) for 15 min (2 mL/min) followed by liver digestion medium (Thermo Fisher Scientific, #17703034) for 15 min. The liver was removed and dissociated in liver perfusion buffer before filtering through a 100 µm strainer (Thermo Fisher Scientific).

Hepatocytes were washed 3 times with low glucose DMEM (D6046; Sigma-Aldrich, St. Louis, MO) supplemented with 10 mM Hepes (Thermo Fisher Scientific, #15630080), 5% charcoal stripped fetal bovine serum (FBS) (Thermo Fisher Scientific, #12329782) and penicillin/streptomycin (50 U/mL; 50 µg/mL).

Hepatocytes viability was determined by the trypan blue exclusion assay and a viability of > 90% was routinely observed. Hepatocytes were seeded at a final density of 2.5×10^5 cells/well onto type I collagen coated 12-well plates in attachment medium (William's E media, #12551032, Thermo Fisher Scientific, 10% FBS, penicillin/streptomycin (50 U/mL; 50 µg/mL), and 10 nM insulin (Sigma-Aldrich, # I9278). The medium was changed 2 h after plating to O/N media consisting of Medium 199 (Thermo Fisher Scientific, #31150022), 5% FBS, penicillin/streptomycin (50 U/mL; 50 µg/mL) and 1 nM insulin. All experiments were performed on the second day.

4.3.4. Transfection and Luciferase assays

For dose-response and specificity assays, COS-1 cells were seeded at density 7×10^4 cells/well in 24-well plates. After 18–24 h, cells were transfected with 0.1 µg GAL4-DBD-NR-LBD expression plasmids, 0.2 µg 5 × UAS-SV40 Firefly Luciferase reporter plasmid, and 0.05 µg Renilla Luciferase-coding internal control (pRL-CMV) plasmid, or 0.2 µg full-length PPAR and RXR-expressing plasmids, with 0.2 µg of any of the CPT1A- or PLIN1-driven reporters, and 0.05 µg pRL-CMV. Transfections were carried out using Lipofectamine® 2000 reagent (Invitrogen, #11668). After 6 hours, the cells were treated with either ADAM, PIRI, or ROSI in DMSO (final concentration of 0.1 %).

After 18 hours of incubation, cells were washed with PBS and lysed in Passive Lysis Buffer (Promega, Madison, WI). Dual-Luciferase® Reporter Assays (Promega, #E1960) were run on a Synergy 2 plate reader (BioTek® Instruments, Winooski, VT) according to manufacturer's manual. Readings of Firefly Luciferase were normalized to the Renilla Luciferase readings, and data from at least three independent transfections experiments run in quadruplicates are presented.

4.3.5. Cytotoxicity assays

Two assays were performed to evaluate the compounds cytotoxic effects. The LDH Cytotoxicity assay measure Lactate dehydrogenase (LDH) leaking from damaged or lysed cells into cell media, while the XTT-based Cell Viability assay is based on measurement of ubiquinone cycle activity as part of the electron transport chain of viable cells. The assays were performed with COS1 cells using the Cytotoxicity Detection Kit (LDH) (Roche, #11644793001) and the In Vitro Toxicology Assay Kid (XTT based) (Sigma-Aldrich, #TOX2-1KT) according to manufacturer's manuals. Absorbance were read using Synergy H1 Hybrid Multi-Mode Microplate Reader (Biotek® Instruments) at 492/750 and 450/690 nm for the LDH and XTT assay, respectively.

4.3.6. Real-time quantitative PCR

RNA was isolated using the RNeasy® Mini kit (Qiagen, #74104) according to the manufacturers manual with following modifications: Lysates from cells with high fat content, e.g. SGBS cells after differentiation, were mixed 1:1 with 70 % ethanol in high salt solution (0.45 M NaCl/0.24 M Na-acetate), before applied to the columns. DNase digestion was performed on-column before washing and eluting of RNA. Isolated RNA (500 ng) was reverse transcribed into cDNA using the High Capacity cDNA Reverse Transcription kit (AppliedBiosystems™, #4368814) according to manufacturer's manual in a total volume of 20 µL per reaction.

Real-time quantitative PCR (qPCR) was performed with 2.5 µL diluted cDNA, equivalent to 12.5 ng RNA, in a 10 µL reaction mix using Kapa SYBR FAST qPCR Master Mix Universal (KapaBiosystems, #KK4601) on a Bio-Rad CFX96 Touch™ Real-Time PCR Detection System (Bio-Rad Laboratories). The gene expression was normalized to TATA-binding protein (*TBP*), and relative mRNA expression levels were calculated by the comparative threshold method.

Assay primers were designed with Primer-BLAST software (NCBI, Bethesda, MD, USA). Primer sequences are listed in Table S1 and S2 (Supporting information).

4.3.7. Staining of neutral lipids

Cells were washed with PBS, fixed in 4 % paraformaldehyde in PBS for 15 minutes, washed with PBS and dH_2O, and stained with Oil Red O working solution (0.3 % Oil Red O (Sigma-Aldrich, #O0625) in 60 % isopropanol) for 15 minutes. After staining, cells were washed with dH_2O and PBS. The stained cells were inspected and photographed with an Olympus® CKX41 inverted microscope (Olympus, Hamburg, Germany) equipped with a ColorView Illu light microscope CCD camera (Olympus) and cell* imaging software v.3.4 (Olympus). All images were processed using Adobe Photoshop CS6 (Adobe Systems Inc, San Jose California, USA).

4.3.8. Statistical analysis

Statistical analysis were performed using GraphPad Prism 6 (GraphPad Software Inc., San Diego, CA, USA). Statistical differences between groups were analysed as specified in the Figure legends. Alpha levels were set to 0.05 for all analyses.

4.4. Docking studies

The Internal Coordinate Mechanics (ICM) program[50] was used for docking of ADAM, OFAI and OFAII into the ligand binding domain (LBD) of PPARα and PPARγ. The LBDs were kept rigid while the compounds were free to move during docking. Compounds were docked into several LBD X-ray structures, to account for conformational differences of the binding pocket seen with co-crystallization of structurally diverse ligands. For PPARγ docking, the X-ray structures (PDB entries) 2VSR, 2VST, 2VV0, 2VV1 and 2VV4 were used, while the PPARα docking were performed with the 2P54 and 3G8I X-ray structures. Prior to docking, crystallographic water molecules, ions and the co-crystallized agonist were removed, while hydrogen atoms were added and optimized using the ECEPP/3 force field. The compounds were built using ICM and optimized before docking. Grid maps that included amino acids within 5 Å of the co-crystallized agonists in the LBD-agonist complexes with a grid spacing of 0.5 Å were calculated before docking. Ligand conformer sampling *in vacuo* and Monte Carlo global energy optimization were used to generate docking poses.[51] The obtained docking poses were scored using the Virtual Ligand Screening (VLS) module of the ICM program. The VLS scoring function uses steric, entropic, hydrogen bonding, hydrophobic and electrostatic terms to calculate the score and also includes a correction term proportional to the number of atoms in the ligand to avoid bias towards larger ligands.[52] Each docking was run in three parallels.

Funding

This work was funded by the Norwegian Research Council through the following grants; BIOTEK 2021 208452/010 (T.S. and S.M.P) and FRIPRO-FRINATEK 230,470 (T.V.H).

Declaration of Competing Interest

The authors declare no competing financial interest.

Acknowledgement

The authors would like to thank Christin Lucas for exceptional technical assistance, and members of the Sæther, Nebb, Hansen, and Matthews research groups for scientific discussions.

Appendix A. Supplementary data

Supplementary data to this article can be found online at https://doi.org/10.1016/j.bmc.2019.07.032. These data include MOL files and InChiKeys of the most important compounds described in this article.

References

1. Krey G, Braissant O, L'Horset F, et al. Fatty acids, eicosanoids, and hypolipidemic agents identified as ligands of peroxisome proliferator-activated receptors by coactivator-dependent receptor ligand assay. *Mol Endocrinol (Baltimore, Md).* 1997;11(6):779–791.
2. Gronemeyer H, Gustafsson JA, Laudet V. Principles for modulation of the nuclear receptor superfamily. *Nat Rev Drug Discovery.* 2004;3(11):950–964.
3. Berger J, Moller DE. The mechanisms of action of PPARs. *Annu Rev Med.* 2002;53:409–435.
4. Nettles KW, Greene GL. Ligand control of coregulator recruitment to nuclear receptors. *Annu Rev Physiol.* 2005;67:309–333.
5. Perissi V, Rosenfeld MG. Controlling nuclear receptors: the circular logic of cofactor cycles. *Nat Rev Mol Cell Biol.* 2005;6:542.
6. Vanden Berghe W, Vermeulen L, Delerive P, De Bosscher K, Staels B, Haegeman G. A paradigm for gene regulation: inflammation, NF-kappaB and PPAR. *Adv Exp Med Biol.* 2003;544:181–196.
7. Varga T, Czimmerer Z, Nagy L. PPARs are a unique set of fatty acid regulated transcription factors controlling both lipid metabolism and inflammation. *BBA.* 2011;1812(8):1007–1022.
8. Wahli W, Michalik L. PPARs at the crossroads of lipid signaling and inflammation. *Trend Endocrinol Metabol TEM.* 2012;23(7):351–363.
9. Braissant O, Foufelle F, Scotto C, Dauca M, Wahli W. Differential expression of peroxisome proliferator-activated receptors (PPARs): tissue distribution of PPAR-alpha, -beta, and -gamma in the adult rat. *Endocrinology.* 1996;137(1):354–366.
10. Ferre P. The biology of peroxisome proliferator-activated receptors: relationship with lipid metabolism and insulin sensitivity. *Diabetes.* 2004;53(Suppl 1):S43–S50.
11. Dalen KT, Schoonjans K, Ulven SM, et al. Adipose tissue expression of the lipid droplet-associating proteins S3–12 and perilipin is controlled by peroxisome proliferator-activated receptor-gamma. *Diabetes.* 2004;53(5):1243–1252.
12. Chawla A, Schwarz EJ, Dimaculangan DD, Lazar MA. Peroxisome proliferator-activated receptor (PPAR) gamma: adipose-predominant expression and induction early in adipocyte differentiation. *Endocrinology.* 1994;135(2):798–800.
13. Mandard S, Muller M, Kersten S. Peroxisome proliferator-activated receptor alpha target genes. *Cell Mol Life Sci: CMLS.* 2004;61(4):393–416.
14. Barrero MJ, Camarero N, Marrero PF, Haro D. Control of human carnitine palmitoyltransferase II gene transcription by peroxisome proliferator-activated receptor through a partially conserved peroxisome proliferator-responsive element. *Biochem J.* 2003;369(Pt 3):721–729.
15. Ruotolo G, Howard BV. Dyslipidemia of the metabolic syndrome. *Curr Cardiol Rep.* 2002;4(6):494–500.
16. Einarson TR, Acs A, Ludwig C, Panton UH. Prevalence of cardiovascular disease in type 2 diabetes: a systematic literature review of scientific evidence from across the world in 2007–2017. *Cardiovasc Diabetol.* 2018;17(1) 83-83.
17. Tenenbaum A, Fisman EZ. Fibrates are an essential part of modern anti-dyslipidemic arsenal: spotlight on atherogenic dyslipidemia and residual risk reduction. *Cardiovasc Diabetol.* 2012;11:125.
18. Knopp RH, Walden CE, Warnick GR, Albers JJ, Ginsberg J, McGinnis BM. Effect of fenofibrate treatment on plasma lipoprotein lipids, high-density lipoprotein cholesterol subfractions, and apolipoproteins B, AI, AII, and E. *Am J Med.* 1987;83(5b):75–84.
19. Robins SJ, Collins D, Wittes JT, et al. Relation of gemfibrozil treatment and lipid levels with major coronary events: VA-HIT: a randomized controlled trial. *JAMA.* 2001;285(12):1585–1591.
20. Fruchart JC, Staels B, Duriez P. PPARS, metabolic disease and atherosclerosis. *Pharmacol Res.* 2001;44(5):345–352.
21. Barbier O, Torra IP, Duguay Y, et al. Pleiotropic Actions of Peroxisome Proliferator-Activated Receptors in Lipid Metabolism and Atherosclerosis. *Arterioscler Thromb Vasc Biol.* 2002;22(5):717–726.
22. Rigamonti E, Chinetti-Gbaguidi G, Staels B. Regulation of macrophage functions by PPAR-alpha, PPAR-gamma, and LXRs in mice and men. *Arterioscler Thromb Vasc Biol.* 2008;28(6):1050–1059.
23. Hedrington MS, Davis SN. Peroxisome proliferator-activated receptor alpha-mediated drug toxicity in the liver. *Expert Opin Drug Metab Toxicol.* 2018;14(7):671–677.
24. Ferri N, Corsini A, Sirtori C, Ruscica M. PPAR-alpha agonists are still on the rise: an update on clinical and experimental findings. *Expert Opin Invest Drugs.* 2017;26(5):593–602.
25. Liu Z-M, Hu M, Chan P, Tomlinson B. Early investigational drugs targeting PPAR-α for the treatment of metabolic disease. *Expert Opin Invest Drugs.* 2015;24(5):611–621.
26. Moldes-Anaya A, Saether T, Uhlig S, et al. Two isomeric C16 Oxo-fatty acids from the diatom chaetoceros karianus show dual agonist activity towards human peroxisome proliferator-activated receptors (PPARs) alpha/gamma. *Marine drugs.* 2017;15(6).
27. Saether T, Paulsen SM, Tungen JE, et al. Synthesis and biological evaluations of marine oxohexadecenoic acids: PPARalpha/gamma dual agonism and anti-diabetic target gene effects. *Eur J Med Chem.* 2018;155:736–753.
28. Egawa D, Itoh T, Yamamoto K. Characterization of covalent bond formation between PPARγ and oxo-fatty acids. *Bioconjug Chem.* 2015;26(4):690–698.
29. Egawa D, Itoh T, Akiyama Y, Saito T, Yamamoto K. 17-OxoDHA Is a PPARα/γ Dual Covalent Modifier and Agonist. *ACS Chem Biol.* 2016;11(9):2447–2455.
30. Kaupang Å, Laitinen T, Poso A, Hansen TV. Structural review of PPARγ in complex with ligands: Cartesian- and dihedral angle principal component analyses of X-ray crystallographic data. *Proteins Struct Funct Bioinf.* 2017;85(9):1684–1698.
31. Chrisman IM, Nemetchek MD, de Vera IMS, et al. Defining a conformational ensemble that directs activation of PPARγ. *Nat Commun.* 2018;9(1):1794.
32. Wabitsch M, Brenner RE, Melzner I, et al. Characterization of a human preadipocyte cell strain with high capacity for adipose differentiation. *Int J Obes Relat Metab Disord.* 2001;25(1):8–15.
33. Lee JY, Hashizaki H, Goto T, Sakamoto T, Takahashi N, Kawada T. Activation of peroxisome proliferator-activated receptor-alpha enhances fatty acid oxidation in human adipocytes. *Biochem Biophys Res Commun.* 2011;407(4):818–822.
34. Brun RP, Tontonoz P, Forman BM, et al. Differential activation of adipogenesis by multiple PPAR isoforms. *Genes Dev.* 1996;10(8):974–984.
35. Takahashi H, Sanada K, Nagai H, et al. Over-expression of PPARα in obese mice adipose tissue improves insulin sensitivity. *Biochem Biophys Res Commun.* 2017;493(1):108–114.
36. Hiuge A, Tenenbaum A, Maeda N, et al. Effects of peroxisome proliferator-activated receptor ligands, bezafibrate and fenofibrate, on adiponectin level. *Arterioscler Thromb Vasc Biol.* 2007;27(3):635–641.
37. Goto T, Lee JY, Teraminami A, et al. Activation of peroxisome proliferator-activated receptor-alpha stimulates both differentiation and fatty acid oxidation in adipocytes. *J Lipid Res.* 2011;52(5):873–884.
38. Tontonoz P, Nagy L, Alvarez JGA, Thomazy VA, Evans RM. PPARγ promotes monocyte/macrophage differentiation and uptake of oxidized LDL. *Cell.* 1998;93(2):241–252.
39. Nagy L, Tontonoz P, Alvarez JGA, Chen H, Evans RM. Oxidized LDL regulates macrophage gene expression through ligand activation of PPARγ. *Cell.* 1998;93(2):229–240.
40. Itoh T, Fairall L, Amin K, et al. Structural basis for the activation of PPARγ by oxidized fatty acids. *Nature Structural &Amp. Mol Biol.* 2008;15:924.
41. Taketa K, Matsumura T, Yano M, et al. Oxidized low density lipoprotein activates peroxisome proliferator-activated receptor-alpha (PPARalpha) and PPARgamma through MAPK-dependent COX-2 expression in macrophages. *J Biol Chem.* 2008;283(15):9852–9862.
42. Fujimori K. Prostaglandins as PPAR Modulators in Adipogenesis. *PPAR Res.* 2012;2012:8.
43. Minnich A, Tian N, Byan L, Bilder G. A potent PPARalpha agonist stimulates mitochondrial fatty acid beta-oxidation in liver and skeletal muscle. *Am J Physiol Endocrinol Metabol.* 2001;280(2):E270–E279.
44. Hardwick JP, Osei-Hyiaman D, Wiland H, Abdelmegeed MA, Song B-J. PPAR/RXR regulation of fatty acid metabolism and fatty acid omega-hydroxylase (CYP4) isozymes: implications for prevention of lipotoxicity in fatty liver disease. *PPAR Res.* 2009;2009 952734-952734.
45. Honkakoski P, Negishi M. Regulation of cytochrome P450 (CYP) genes by nuclear receptors. *Biochem J.* 2000;347(Pt 2):321–337.
46. Gim HJ, Choi Y-S, Li H, Kim Y-J, Ryu J-H, Jeon R. Identification of a novel PPAR-γ agonist through a Scaffold tuning approach. *Int J Mol Sci.* 2018;19(10):3032.
47. Tsakovska I, Al Sharif M, Alov P, et al. Molecular modelling study of the PPARγ receptor in relation to the mode of action/adverse outcome pathway framework for liver steatosis. *Int J Mol Sci.* 2014;15(5):7651–7666.
48. Weedon-Fekjaer MS, Dalen KT, Solaas K, Staff AC, Duttaroy AK, Nebb HI. Activation of LXR increases acyl-CoA synthetase activity through direct regulation of ACSL3 in human placental trophoblast cells. *J Lipid Res.* 2010;51(7):1886–1896.
49. Napal L, Marrero PF, Haro D. An intronic peroxisome proliferator-activated receptor-binding sequence mediates fatty acid induction of the human carnitine palmitoyltransferase 1A. *J Mol Biol.* 2005;354(4):751–759.
50. Abagyan R, Totrov M, Kuznetsov D. ICM—A new method for protein modeling and design: applications to docking and structure prediction from the distorted native conformation. *J Comput Chem.* 1994;15(5):488–506.
51. Abagyan R, Kufareva I. The flexible pocketome engine for structural chemogenomics. *Method Mol Biol (Clifton, NJ).* 2009;575:249–279.
52. Schapira M, Abagyan R, Totrov M. Nuclear hormone receptor targeted virtual screening. *J Med Chem.* 2003;46(14):3045–3059.